HHS Public Access

Author manuscript

Nat Struct Mol Biol. Author manuscript; available in PMC 2011 March 01.

Published in final edited form as:

Nat Struct Mol Biol. 2010 September ; 17(9): 1088–1095. doi:10.1038/nsmb.1869.

Mycobacterium tuberculosis lipoprotein LprG (Rv1411c) binds triacylated glycolipid agonists of Toll-like receptor 2

Michael G. Drage[1,6], **Han-Chun Tsai**[4,6], **Nicole D. Pecora**[1,6], **Tan-Yun Cheng**[5], **Ahmad R. Arida**[1,2], **Supriya Shukla**[1], **Roxana E. Rojas**[3], **Chetan Seshadri**[5], **D. Branch Moody**[5], **W. Henry Boom**[3,7], **James C. Sacchettini**[4,7], and **Clifford V. Harding**[1,7]

[1] Department of Pathology, Case Western Reserve University/University Hospitals Case Medical Center, Cleveland, OH 44106-7288, USA

[2] Department of Biochemistry, Case Western Reserve University/University Hospitals Case Medical Center, Cleveland, OH 44106-7288, USA

[3] Division of Infectious Diseases and Tuberculosis Research Unit, Case Western Reserve University/University Hospitals Case Medical Center, Cleveland, OH 44106-7288, USA

[4] Department of Biochemistry and Biophysics, Texas A&M University, College Station, Texas 77843-2128, USA

[5] Division of Rheumatology, Immunology and Allergy, Brigham and Women's Hospital, Harvard Medical School, Boston, MA, USA

Abstract

Knockout of *lprG* results in decreased virulence of *Mycobacterium tuberculosis* (Mtb) in mice. Mtb lipoprotein LprG has TLR2 agonist activity, thought to be dependent on its N-terminal triacylation. Surprisingly, here we find that non-acylated LprG retains TLR2 activity. Moreover, we show LprG association with triacylated glycolipid TLR2 agonists lipoarabinomannan, lipomannan and phosphatidylinositol mannosides (which share core structures). Binding of triacylated species was specific to LprG (not LprA) and increased LprG TLR2 agonist activity; conversely, association of glycolipids with LprG enhanced their recognition by TLR2. The crystal structure of LprG in complex with phosphatidylinositol mannoside revealed a hydrophobic pocket that accommodates the three alkyl chains of the ligand. In conclusion, we demonstrate a glycolipid binding function of LprG that enhances recognition of triacylated Mtb glycolipids by TLR2 and may affect glycolipid assembly or transport for bacterial cell wall biogenesis.

Communicating author: Clifford V. Harding, Department of Pathology, Case Western Reserve University/University Hospitals Case Medical Center, 2103 Cornell Ave, Cleveland, OH 44106-7288, USA. Phone: 216-368-5059. FAX: 216-368-0494. cvh3@cwru.edu.

[6]Joint first authors

[7]Joint senior authors

Author Contributions

M.G.D., H.-C.T., N.D.P, T.-Y.C, A.R.A., R.E.R and C.S., design, performance and interpretation of experiments, manuscript preparation; D.B.M., W.H.B, J.C.S. and C.V.H, design and interpretation of experiments, manuscript preparation.

Database Accession Numbers

The pdb accession codes are 3MHA (LprG-PIM), 3MH9 (LprG_V91W) and 3MH8 (LprG).

Keywords

Toll-like receptor 2; lipoprotein; glycolipid; Mycobacterium tuberculosis

Mycobacterium tuberculosis (Mtb) infects one third of the world's population and continues to be a leading cause of death. Although immune responses by immunocompetent individuals can contain infection, sterilizing immunity is not usually achieved [1]. Infected individuals harbor latent disease with the potential for future reactivation, clinical disease, infectious spread and mortality.

The hydrophobic cell envelope of Mtb may be involved in several aspects of tuberculosis pathogenesis, including long-term survival in the host. Mtb cell wall components stimulate host responses and contribute to the activity of Freund's adjuvant [2]. The mycobacterial cell wall contains glycolipids, which contribute to resistance to bactericidal free-radicals [3] and modulate immune functions, including phagosome maturation [4,5] and cytokine production. The cell wall also contains an abundance of N-terminally triacylated lipoproteins [6,7]. Four small homologous lipoproteins (LprG, LprA, LppX and LprF), only found in the suborder of *Corynebacterineae*, contain a signal peptide for secretion through the Sec system and a lipobox motif for lipid modification on a conserved cysteine. Diacylglycerol is linked by a thioester bond to the cysteine, and a third acyl chain is attached by an amide bond to the amino group of the cysteine, resulting in triacylation. These lipoproteins are predicted to be localized to the periplasm or cell wall, e.g. anchored to the outer leaflet of the cell membrane through their acyl chains. LprG (Rv1411c) may function with the other protein in its operon, a membrane pump (Rv1410c). Knockout of the LprG or its operon results in attenuated growth and survival in mice and macrophages [8–10]. Deletion of the LprG operon in *Mycobacterium smegmatis* results in decreased sliding motility and altered cell morphology [11], suggesting that LprG function may be related to cell wall biosynthesis. LppX has also been proposed to be involved in cell wall biosynthesis by binding and transporting phthiocerol dimycocerosate (PDIM) [12].

Toll-like receptor 2 (TLR2), which forms heterodimers with TLR1 or TLR6, is an important contributor to innate immune recognition of Mtb [13–23]. TLR2/TLR1 heterodimers bind triacylated lipopeptides. TLR2 agonist activity has been demonstrated for the following Mtb lipoproteins (Mtb H37Rv gene nomenclature and protein name synonyms in parentheses): LpqH (*Rv3763*, 19-kD lipoprotein) [18–21], LprA (*Rv1270c*) [23], LprG (*Rv1411c*, p27) [24], and Psts1 (*Rv0934*; PhoS1, p38) [25]. Mycobacterial agonists of TLR2 also include glycolipids, e.g. phosphatidyl-(myo)-inositol mannosides (PIMs), lipomannans (LMs), lipoarabinomannans (LAMs), and inositol phosphate-capped LAMs (PI-LAMs) [13,14,22].

We investigated the structural basis of TLR2 agonist activity of Mtb LprG. Crystal structures show that the thioether-linked diacylglycerol binds a hydrophobic pocket in TLR2, and the amide-linked third acyl chain binds TLR1 [26]. Surprisingly, our studies showed that nonacylated (NA)-LprG retains TLR2 stimulatory capacity, and the crystal structure of NA-LprG revealed a glycolipid binding pocket lined with hydrophobic residues that could accommodate lipids with three acyl chains. This pocket non-covalently binds triacylated glycolipids, and introduction of a single point mutation in this pocket blocks the

glycolipid binding function of LprG. We propose that LprG functions in mycobacteria as a carrier of glycolipids during their trafficking and delivery to the mycobacterial cell wall, contributing to virulence [8,11] and providing potential opportunities for targeting in drug design. In addition, the glycolipid carrier function of LprG may facilitate recognition of triacylated glycolipids by TLR2.

Results

LprG carries a mycobacterial TLR2 agonist

In the prolipoprotein maturation pathway, N-terminal acylation of a cysteine results in a lipoprotein capable of inducing a potent TLR2 response. To determine the importance of N-terminal acylation to TLR2 agonist activity, we compared the TLR2 agonist activity of two homologous Mtb lipoproteins, LprG and LprA, with and without N-terminal triacylation. These lipoproteins are predicted to be similarly acylated by a common enzymatic pathway [27] and, therefore, to have similar TLR2 activity, yet acylated LprG induced TLR2-dependent IL-8 secretion with more than 10-fold greater potency than acylated LprA in a bioassay with HEK293 cells transfected to express TLR2 and CD14 (Fig. 1A) or TLR2 alone (data not shown). Accordingly, we designed non-acylated (NA) forms with the signal peptide removed and the N-terminal cysteine replaced with methionine to investigate whether structures other than the acyl chains could affect TLR2 agonist activity. Recombinant His_6-tagged acylated and NA versions of Mtb LprA and Mtb LprG were expressed in *Mycobacterium smegmatis* and assessed for TLR2 agonist activity. Consistent with prior data [23], NA-LprA lacked TLR2 activity, indicating that acylation of LprA was essential for its TLR2 activity (Fig. 1A). In contrast, NA-LprG retained significant TLR2 activity (Fig. 1A), showing that LprG possesses a previously unknown determinant of TLR2 agonist activity independent of its N-terminal acylation.

NA-LprG had substantially reduced activity when expressed in *E. coli* instead of *M. smegmatis* (Fig. 1B), suggesting that LprG may carry TLR2 agonist(s) that are present in mycobacteria but not *E. coli*. Furthermore, TLR2 activity of NA-LprG purified from *E. coli* was significantly increased following incubation with a lysate of *M. smegmatis* (Fig. 1B), Mtb H37Ra (Fig. 1C) or Mtb H37Rv (Fig. 1C). In contrast, NA-LprA purified from *E. coli* did not acquire TLR2 activity from mycobacterial lysates (Fig. 1B, C). These results demonstrate that NA-LprG binds a mycobacterial TLR2 agonist and can deliver it for recognition by TLR2.

LprG has a hydrophobic binding pocket for TLR2 agonists

Crystals were produced for a truncation form of NA-LprG lacking N-terminal residues 1-35 (i.e. the signal peptide and the triacylated cysteine) and C-terminal residues 232-236 (secondary structure prediction indicated random coils for these sequences). This NA-LprG construct was a monomer in solution as determined by gel filtration (isolated as a single peak of ~22 kDa). Crystals were found to be in the C2 space group. The structure was solved using MAD methods and refined to a resolution of 2.0 Å with two molecules in the asymmetry unit (Table 1). Both molecules (A and B) have large hydrophobic cavities with distinct entry portals.

The overall LprG structure consists of a single domain in an α/β fold with a β-sheet composed of 10 anti-parallel strands on one side and 6 α-helices on the opposite side. Between the β-sheet and α-helices is a large cavity (~1500 Å^3) (Fig. 2A). The entrance to the cavity is approximately 9 Å × 20 Å and lies near β3, β4 and β5. The lower part of the molecule as positioned in Fig. 2A is a twisted β-sheet (β6, β7, β8, β9 and β10) at the end of the cavity with a narrow binding channel (Fig. 2A, B). In the central portion of the cavity, the β-sheet's concave face is towards the α-helices, forming the large cavity. The cavity and the portal are lined primarily with the side chains of hydrophobic residues (Fig. 2B), which supports the hypothesis that LprG can bind lipids in the cavity.

Mutation of the pocket blocks association of TLR2 agonists

We designed a site-directed mutant of LprG in which valine 91, located at the portal, was replaced with a bulkier tryptophan that was predicted to partially occlude the binding cavity (Fig. 3). Mutant NA-LprG-V91W was expressed in *M. smegmatis* and crystallized. The overall RMSD between wildtype NA-LprG and mutant NA-LprG-V91W is ~1.0 Å, and the Luzzati coordination mean error is ~0.2 Å. The crystal structure of NA-LprG-V91W showed that tryptophan 91 shifted the portal wall inward by 3.5 Å compared to the wild type (Fig. 3, Table 1). The region between leucine 73-leucine 76 was also shifted into the cavity by 0.5 Å to form van der Waals interactions with tryptophan 91, further narrowing the portal. The loop between s3 and s4 and the loop between s5 and helix α2 were also relocated by approximately 2 Åfrom the entrance in response to the presence of the indole ring. Due to movement of these loops and the tryptophan mutation, the mutation reduced the size of the cavity entrance from 9 Å × 20 Å to 8 Å × 13 Å. The resulting cavity volume of NA-LprG-V91W (1200Å^3) was significantly smaller than that of NA-LprG (1500Å^3). Thus, as predicted, the V91W mutation reduced the dimensions of the pocket entrance dimensions and the volume of the cavity.

The narrowed cavity entrance and smaller cavity of NA-LprG-V91W were predicted to provide steric hindrance to limit substrate binding. Consistent with this hypothesis, NA-LprG-V91W had substantially reduced TLR2 agonist activity relative to NA-LprG (Fig. 3). Mutations at two other sites in the hydrophobic pocket (V194R and V217F) also decreased TLR2 agonist activity of NA-LprG (data not shown). Furthermore, when NA-LprG-V91W was expressed in *E. coli*, purified and then incubated with a lysate of *M. smegmatis* or Mtb, the V91W mutant lacked the ability to acquire TLR2 agonist activity from mycobacteria (Fig. 3). These results indicated that the hydrophobic cavity is a binding site for TLR2 agonist(s), which are delivered by LprG for recognition by TLR2.

Mycobacterial glycolipids are associated with LprG

NA-LprG was found to signal through TLR2/TLR1 heterodimers (Fig. S-1), a pattern observed with mycobacterial glycolipids including LAM (Fig. S-1) [16] and LM (Fig. S-1) [15], as well as triacylated lipopeptide (Fig. S-1). To identify its associated TLR2 agonists, NA-LprG was purified from *M. smegmatis* by Ni-affinity and anion-exchange chromatography, and subjected to polyacrylamide gel electrophoresis (Fig. 4). Silver stain and anti-His_6 Western blot of NA-LprG, NA-LprG-V91W or NA-LprA showed a single band at approximately 24 kDa (Fig. 4A and data not shown). Staining of carbohydrates after

periodate oxidation showed additional bands that comigrated with protein molecular weight markers of 25–35 kDa, 14-18 kDa and <10 kDa (Fig. 4B), which corresponded roughly to the expected positions of LAM, LM and PIM, respectively, and were found to comigrate with authentic glycolipid standards (Fig. 4D and data not shown). These bands likely represent glycolipids because they were seen after periodate oxidation but not on conventional silver stain, and glycolipids in the PIM-LAM series resolve as broad bands based on heterogeneity of the arabinan and mannan components in each molecular species. Importantly, LAM and LM were associated with NA-LprG but not NA-LprG-V91W or LprA, indicating that these glycolipid agonists of TLR2 are associated preferentially with NA-LprG. Association of PIM was detected with NA-LprG, to a lesser degree with NA-LprA, and only minimally with NA-LprG-V91W. Western blot with polyclonal anti-*M. bovis* BCG antibody revealed bands consistent with LAM, LM and PIM in association with NA-LprG but not NA-LprG-V91W or NA-LprA (Fig. 4C; anti-BCG staining may detect only a subset of PIM species). Furthermore, Western blot with a LAM-specific monoclonal antibody confirmed association of LAM with NA-LprG and its absence from NA-LprG-V91W and NA-LprA (Fig. 4D).

LAM, LM, and PIM share a common structural core, suggesting that they all associate with NA-LprG via this shared structural motif, which may also contribute to TLR2 agonist activity. To determine the structures of small molecules associated with NA-LprG and related proteins, methanol was used to denature proteins and allow detection of protein-associated small molecules with mass to charge (m/z) ratio up to 2000 by nanoelectrospray ionization mass spectrometry. Methanol alone (Fig. 4E) or methanol elutes of an unrelated protein, Pab C (Fig. S-2), did not give detectable ions. In contrast, NA-LprG expressed in *M. smegmatis* yielded ions corresponding to mycobacterial phospholipids (Figs. 4E and S-2). Ions detected at *m/z* 851.4, 1013.5, 1175.5 and 1413.7 corresponded to the expected masses of diacyl phosphatidylinositol, diacyl phosphatidylinositol monomannoside (PIM_1), diacyl phosphatidylinositol dimannoside (PIM_2) and triacyl PIM_2 (Ac_1PIM_2), respectively. Collision induced dissociation mass spectrometry (CID-MS) yielded product ions expected from these proposed structures, confirming assignments based on mass alone (Figs. 4E and S-2). For example, Ac_1PIM_2 (*m/z* 1413.7) yielded products expected from the loss of mannose (*m/z* 1251), loss of acyl mannose (*m/z* 1013), loss of C16:0 acyl (*m/z* 1157), loss of C19:0 fatty acyl (*m/z* 1115) and acyl phosphoinositol dimannoside (*m/z* 803). Thus, LprG binds at least four structurally related molecules that all contain phosphatidylinositol as the core structure but differ in the number of mannose units and fatty acyl chains.

Liquid chromatography-mass spectrometry (LC-MS) was used to compare mass spectral signals of individual molecular species eluted from the same molar quantity of NA-LprG, NA-LprG-V91W or NA-LprA (Fig. 4F-I). Total ion current was used as a control to confirm comparable input of protein (Fig. 4F), and signals were monitored simultaneously in narrow ranges (+/− 0.5 amu) near the expected masses of diacyl PI (Fig. 4G), diacyl PIM_1 (Fig. 4H) and Ac_1PIM_2 (Fig. 4I). Diacyl PI and diacyl PIM_1 were associated with NA-LprG and NA-LprA, but only in lower amounts with NA-LprG-V91W. In contrast, triacylated Ac_1PIM_2 was only associated with NA-LprG. Whereas LprA binds only diacylated PIMs, LprG binds both diacylated and triacylated PIMs. Because a large proportion of LAM is triacylated [28],

the preferential ability of LprG to bind triacylated PIMs likely explains the greater association of LAM with LprG relative to LprA.

There are no known differences between *M. smegmatis* and Mtb with regard to structures of phosphatidylinositol and PIM species. Comparative mass spectral profiling of phospholipids isolated from whole bacteria revealed the following m/z values for abundant molecular species in Mtb vs. *M. smegmatis*, respectively: 851.564 vs. 851.562 for phosphatidylinositol, 1013.66 vs. 1013.64 for PIM_2, and 1413.89 vs. 1413.89 for Ac_1PIM_2. These data reveal no significant differences in structures of phosphatidylinositol or PIM species between *M. smegmatis* and Mtb, suggesting that these glycolipids will similarly associate with LprG in both *M. smegmatis* and Mtb (LprG was cloned from Mtb for these studies).

Structure of Ac_1PIM_2 bound to NA-LprG

To understand the structural basis of glycolipid binding, NA-LprG was incubated with an equimolar mixture of PIM and phosphatidylinositol from *M. smegmatis*. The crystal structure of Ac_1PIM_2 bound to NA-LprG was solved to 1.85 Å resolution (Fig. 5, Table 1). The overall structure of the protein, the electrostatic surface of the complex, and the cavity volume were similar to those of the apo-protein (RMSD of 0.6 Å and cavity volume of 1500Å^3). In the NA-LprG-PIM crystal, one molecule (A) in the asymmetric unit has a triacylated Ac_1PIM_2 bound and the other molecule (B) has nothing bound. While both protein molecules are very similar in structure (RMSD of 1.3Å), molecule B shows a ~2Å movement for the α-helix-loop-α-helix motif at the portal to the Ac_1PIM_2 binding site. The movement of this α-helix-loop-α-helix motif (Asp94 to Gln106) re-positions the side chain of Tyr102 approximately 3 Å where it sterically prohibits Ac_1PIM_2 binding. The movements are not influenced by crystal packing as the apo-protein has nearly identical crystal packing.

Triacylated Ac_1PIM_2 (C19:0, C16:0, C16:0) was resolved in the binding cavity of molecule A (Fig. 5A,C). The interactions between LprG and Ac_1PIM_2 were mainly through van der Waals contacts between the hydrophobic side chains within the cavity and the three acyl chains of the ligand. The deepest part of the cavity, where the mannosyl C16 chain is located, appears to be capable of accommodating an acyl chain that is at least two more carbons in length (Fig. 5A). The sugar moieties of Ac_1PIM_2 were found on the edge of the entry portal, directly outside the cavity. The α-helix-loop-α-helix region occupies about half of the LprG cavity entrance, very close to where mannosyl inositol binds in molecule A. This region is negatively charged (Fig. 5D), providing a favorable environment for sugar binding. However, in the structure of NA-LprG-PIM only two relatively weak interactions between the sugar moieties of Ac_1PIM_2 are observed. They are hydrogen bonds between the backbone oxygen of Gly42 and 4-hydroxy of C16 acyl mannose (~2.7Å), and between the backbone oxygen of Asp100 and phosphate oxygen of the ligand (~3.0Å). Therefore, the major component of ligand recognition involves the hydrophobic residues in the cavity.

Superimposed structures of NA-LprG-V91W mutant and NA-LprG-PIM revealed that tryptophan 91 overlapped with the C19 acyl chain at the sn1 position of Ac_1PIM_2 (Fig. 5B). Thus, the V91W mutation would occlude binding of Ac_1PIM_2, correlating with decreased

association of Ac_1PIM_2 from mass spectrometry (Figs. 4, 5) and decreased TLR2 activity (Fig. 3).

LprG binds mycobacterial glycolipids that are TLR2 agonists

To directly test the ability of NA-LprG to bind mycobacterial glycolipids, we purified NA-LprG from *E. coli* (with little or no TLR2 activity), incubated it with LM or LAM, re-purified it by Ni-affinity and anion-exchange chromatography, and tested it for TLR2 agonist activity. NA-LprG was able to bind LM and LAM and deliver them for recognition by TLR2 (Fig. 6A, B), but NA-LprG-V91W (Fig. 6A, B) and NA-LprA (data not shown) lacked this ability, consistent with the pattern of LM and LAM association in Fig. 4. Importantly, association with NA-LprG enhanced the apparent potency of LAM and LM by at least 1.5 log orders of magnitude (Fig. 6A, B). This comparison is based on the molar concentrations of NA-LprG shown in Fig. 6, assuming that 100% of the NA-LprG molecules were loaded with LM or LAM. In the likelihood that glycolipid loading was less than 100% efficient, the factor by which association with NA-LprG enhanced glycolipid potency would be higher. We conclude that NA-LprG binds mycobacterial glycolipids and significantly enhances their recognition by TLR2.

Glycolipids contribute to the TLR2 activity of acylated LprG

Our studies indicate existence of two distinct determinants of TLR2 agonist activity of LprG, N-terminal acylation and chaperoned glycolipids. We studied acylated LprG and acylated LprG-V91W to determine the relative contribution of these mechanisms. Acylated LprG-V91W was more than a factor of 10 less potent than acylated LprG (Fig. 6C), indicating that the majority of TLR2 agonist activity of acylated LprG was attributable to carried glycolipid. Consistent with this finding, Western analysis revealed association of LAM with acylated LprG (Supplemental Fig. S-5). Acylated LprG-V91W had potency similar to acylated LprA (Fig. 6C), indicating that TLR2 activity remaining when glycolipids were not associated with LprG was similar to that of LprA, reflecting similar N-terminal acylation of these molecules. Thus, the higher potency of LprG relative to LprA results from LprG-associated glycolipids, which are a major determinant of the overall LprG TLR2 activity.

Discussion

The discovery of a glycolipid carrier function has significant implications for the function of LprG in bacterial physiology. LprG is widely present in mycobacteria with 100% sequence identity among Mtb complex species. LprG (*Rv1411c*) and p55 (*Rv1410c*) are encoded in an operon that is important for virulence [8,11,29]. We propose that LprG serves as a carrier to facilitate assembly or trafficking of glycolipids. The LprG pocket structure confers specificity for binding to triacylated lipids, which are a relatively small pool within the much larger pool of diacylated lipids. Glycolipids have important roles in bacterial physiology and host-pathogen interactions, and a potential future goal is inhibition of these processes by targeting the pocket of LprG with chemotherapeutics.

LprG has a pocket that accommodates three acyl chains, raising the possibility that LprG, like LolA and LolB of *Escherichia* coli, may bind lipopeptides via their triacylated N-termini. LolA and LolB, however, show less than 20% identity to LprG, and their lipid binding cavities are considerably smaller than LprG's. Furthermore, mass spectrometry did not reveal other lipopeptides associated with LprG purified from *M. smegmatis*, possibly due to competition by glycolipid ligands in mycobacteria or potential structural constraints. It is also unlikely that LprG would bind its own acyl peptide without considerable unfolding as the N-terminal side of LprG is ~50 Å away from the binding cavity entrance. These considerations fit with functional data (Fig. 6C) and biochemical data (Supplemental Fig. S-5) that show glycolipid association with both NA-LprG and acylated LprG.

NA-LprG is unique among the studied proteins in its ability to bind Ac_1PIM_2, LM and LAM (Fig. 4), all of which may contain the triacylated PIM core structure that fits within the LprG pocket (Fig. 5). LAM is a complex polymer with a high molecular weight that cannot be analyzed by the MS systems reported here, but other studies show that a large proportion of naturally occurring LAM is triacylated [28]. Therefore, preferential association of LAM with NA-LprG as compared to NA-LprA or NA-LprG-V91W may be explained by acyl chain interactions with the pocket as seen in the NA-LprG-Ac_1PIM_2 crystal structure. These findings are consistent with the observed TLR2/TLR1 dependence of signaling by Mtb glycolipids in the PIM-LM-LAM series [14–17] and the concept that TLR2 activity of these mycobacterial glycolipids requires their triacylation[30].

Recognition of PIM by LprG primarily involves interactions between the hydrophobic cavity of LprG and the three fatty acyl chains of the glycolipid (Fig 5-A, 5-D). We cannot exclude contributions of the longer carbohydrate chains of LM and LAM to LprG binding. Our mass spectrometry data indicate that the structures of PIMs associated with LprG, e.g. Ac_1PIM_2, are similar in Mtb and *M. smegmatis*. LMs and LAMs are formed by additional glycosylation of PIMs. LAM is mannose-capped in Mtb, unlike *M. smegmatis*, and the resulting Man-LAM has lower TLR2 potency than PI-LAM from *M. smegmatis*, but Mtb LAM has significant TLR2 agonist activity. Furthermore, the ability of Mtb lysate to efficiently "charge" LprG with TLR2 activity (Fig. 1C) indicates that Mtb glycolipids are an effective source of LprG-chaperoned TLR2 agonist.

The binding pocket of TLR2 is hydrophobic with a volume of 1800 Å3, close to that of the LprG binding pocket, but contains only two acyl chains of lipopeptides [26,31] and glycolipids [31], perhaps due to a restricted entrance. The third acyl chain of triacylated glycolipids may bind TLR1 [26]. Thus, the triacyl structure that provides specificity for binding to LprG also determines the ability of Mtb glycolipids to signal through TLR2/TLR1. Although LprA does not chaperone triacylated TLR2 agonists, modeling of LprA also reveals a hydrophobic pocket (Supplemental Fig. S-4), and we observed association of diacylated glycolipids with LprA. Another Mtb lipoprotein, LppX, has a hydrophobic pocket [12]. Other mycobacterial lipoproteins may be carriers of hydrophobic ligands, some of which may be TLR2 agonists, and the potential contribution of chaperoned molecules to TLR2 activity of other lipoproteins should be considered.

While the localizations of LprG and NA-LprG remain to be determined, acylated LprG is predicted to traffic to the outer surface of the mycobacterial cell membrane, where LM and LAM are assembled [32]. LprG may contribute to LAM assembly, trafficking and/or insertion into the cell wall. NA-LprG is predicted to be localized to the cytoplasm, as it lacks a signal peptide, and its loading with glycolipids may occur upon bacterial lysis. NA-LprG is a very useful tool to dissect the different components of LprG TLR2 activity, carried glycolipids and N-terminal acylation, but future studies of physiologic functions should focus on acylated LprG.

LprG may enhance TLR2 recognition of Mtb by direct and/or indirect mechanisms. LprG may directly convey glycolipids to host receptors, e.g. TLR2 or CD14. This mechanism implies release of LprG from Mtb, either spontaneously or during phagosomal processing of Mtb, which may allow LprG to reach TLR2 molecules that target to phagosomes. In addition, a role for LprG in the assembly, trafficking and cell wall insertion of glycolipids indicates that LprG may affect the bioavailability of glycolipid TLR2 agonists.

Our results suggest that host cells can co-opt the carrier function of LprG to enhance TLR2 recognition of mycobacterial glycolipids. Association of glycolipids with NA-LprG increased their apparent potency by at least a factor of 1.5 log. To our knowledge this is the first report of a pathogen-derived protein serving as a carrier for delivery of hydrophobic agonists for innate immune recognition. For LPS, another hydrophobic TLR ligand, transfer to TLR4 is enhanced by host-expressed carriers, LPS binding protein [33] and CD14 [34]. LprG may deliver glycolipids to TLR2 via delivery to CD14, which we observed to increase recognition of NA-LprG, presumably by enhancing glycolipid delivery to TLR2.

LprG influences progression of Mtb infection *in vivo*, as genetic deletion of *Rv1411c* (encoding LprG) in Mtb H37Rv reduces virulence of Mtb in C57BL/6 mouse pulmonary aerosol infection models (CFU burden decreases by a factor of 1000 to 10,000 relative to wild type Mtb H37Rv or a strain in which the genetic deletion has been complemented; Niaz Banaei, Stanford University, personal communication). This establishes the importance of LprG to virulence, apparently by its contributions to Mtb cell wall assembly, delivery of glycolipids to TLR2 or both.

Online Methods

Mammalian cell culture and cytokine ELISAs

Bone marrow was obtained from TLR1$^{-/-}$, TLR2$^{-/-}$, TLR6$^{-/-}$, CD14$^{-/-}$, wild-type C57BL/6 and F2 hybrids of C57BL/6 and 129sv mice (see Supplemental Methods). Bone marrow cells were cultured for 7-12 d in standard medium supplemented with 25% LADMAC cell-conditioned medium [35]. HEK293 cells stably expressing TLR2-YFP (HEK293.TLR2) [36,37], HEK293.pcDNA3 cells transfected with the empty vector. HEK293.TLR2-CD14 cells (Invivogen 293-htlr2cd14) or bone marrow-derived macrophages were incubated for 12-16 h with or without TLR2 agonist. IL-8 and TNFα were quantified by ELISA. Synthetic TLR agonists included FSL-1 (Invivogen, tlrl-fsl), Pam_3CSK_4 (Invivogen, tlrl-pms), and CpG-B ODN 1826 (5′-tcc atg acgttc ctg acg tt-3′ lot C44-05225-q1a) provided by Coley Pharmaceutical Group (Wellesley, MA).

Cloning and expression of His_6-tagged proteins

LprA and NA-LprA were cloned previously [23]. LprG was amplified from Mtb H37Rv genomic DNA by PCR,a non-acylated (NA) variant of LprG was cloned by using a 5' primer that excluded the signal sequence and changed the acylated cysteine to a methionine, and site-directed mutagenesis was performed (Supplemental Methods). For expression in *M. smegmatis*, constructs were digested with NdeI and HindIII (NEB, Ipswich, MA) and ligated into the shuttle vector pVV16 (provided byJ. Belisle, Colorado State University, Fort Collins, CO) behind the constitutively active *hsp60* promoter and in-frame with a C-terminal His_6 tag. For expression in *E. coli* Rosetta cells (EMD, Gibbstown, NJ), constructs were digested with NdeI and HindIII and ligated with the expression plasmid pET-22b(+) (Novagen, Madison, WI) (removing the pelB leader sequence), placing the coding sequence behind the IPTG-inducible T7 promoter and in frame with a C-terminal His_6 tag. Conditions for expression of recombinant lipoproteins in *M. smegmatis* and *E. coli* are described in Supplemental Methods.

Purification of His_6-tagged proteins

Bacteria were disrupted mechanically by 4 passages through a French press (2000 psi). Insoluble material was removed from the lysate by ultracentrifugation at 100,000 *g* for 1 h at 4°C. Recombinant lipoproteins were purified from the supernatant by Ni-affinity and anion exchange chromatography (material eluted at 50–200 mM NaCl was used for all experiments, see.Supplemental Methods). Protein purity was verified by SDS-PAGE with silver stain and anti-His_6 Western blot. Both acylated and non-acylated forms were readily soluble in aqueous buffers.

Mycobacterial lysates and charging of E. coli-derived proteins

Lysates of *M. smegmatis* or Mtb H37Ra were prepared by sonication (Supplemental Methods). Mtb H37Rv lysates were obtained from Karen Dobos-Elder and John Belisle, Colorado State University, under NIH contract HHSN266200400091C, N01-AI-40091. For charging of *E. coli*-expressed proteins, 300–500 μg of protein (purified by Ni-affinity and anion-exchange chromatography) was incubated with mycobacterial lysate for 4 h at 37°C. Insoluble material was pelleted, and charged proteins were repurified by Ni-affinity and anion-exchange chromatography. For charging with purified glycolipids, proteins similarly purified from *E. coli* (100 μg) were incubated for 3 h at 37°C with 0.5–50 μg of purified glycolipid (Invivogen, San Diego, CA; LAM-MS, LM-Ms) in a total volume of 100 μl and repurified.

SDS-PAGE and visualization of purified proteins and glycolipids

Gels (13% acrylamide) were cast and run using a Tris-HCl buffer system. Proteins were visualized with Silver Stain Plus (BioRad). Carbohydrates (including glycolipids) were visualized with Pro-Q Emerald 300 (Molecular Probes, Eugene, OR P20495) following periodate oxidation. Mycobacterial proteins and glycolipids were also visualized by Western analysis with rabbit polyclonal anti-BCG (DAKO, Glostrup, Denmark). To compare the amount of LAM normalized to the amount of His_6-tagged protein, two-color Western analysis was performed using the Odyssey Western Analysis System (LI-COR, Lincoln,

NB). Materials were detected by sequential incubations with mouse monoclonal anti-LAM (CS-35, NIAID HHSN266200400091C contract, Colorado State University), polyclonal goat anti-mouse (LI-COR), mouse monoclonal anti-His_6 (Santa Cruz, Santa Cruz, CA) and donkey anti-mouse (LI-COR).

Mass spectrometry and identification of ligands of NA-LprG

For nanospray mass spectrometry, 12 μg of purified protein was denatured in 500 μL methanol, and 10 μL of methanol eluate was analyzed by negative-mode electrospray ionization mass spectrometry (LCQ Advantage, Thermo Finnigan, Ringoes, NJ). For LC-MS analysis, 4.3 nanomoles of each protein was analyzed on a monochrome diol column (46 mm × 250 mm, 3 μm; Varian Inc., Palo Alto, CA) coupled on-line to a LXQ 2 dimensional ion-trap mass spectrometer (Thermo Finnigan) equipped with an electrospray ionization (ESI) source (Supplemental Methods).

Expression and purification of NA-LprG for crystallography studies

Analysis of Mtb LprG by secondary structure prediction and SignalP predicted the N-terminal 35 residues to be a signal peptide and the C-terminal 5 residues to be disordered, so these residues were excluded from LprG coding region (Supplemental Methods). The resulting sequence was ligated into pET30b (Novagen) and transformed into BL21 (DE3) (Novagen) and autotroph *E. coli* B834 (DE3) (Novagen). Cells were disrupted and the lysate was centrifuged at 10,000 *g* for 60 min. LprG was purified by Ni-affinity chromatography and concentrated to 10 mg/mL for crystallization. NA-LprG crystals were obtained from 0.1 M sodium acetate trihydrate, pH 4.5, 25% PEG3350. Se-Met crystals were obtained from 0.1 M Bis-Tris pH 6.5, 25% PEG3350. NA-LprG-V91W crystals were produced in 0.2 M ammonium sulfate, 0.1 M sodium acetate trihydrate, pH 4.6, 30% PEG monomethyl ether 2000. Co-crystallization with glycolipid produced crystals in the NA-LprG crystal condition.

Determination of LprG structures

One 3-wavelength MAD data set was collected to resolution of 1.9 Å (Table 1) at the Lawrence Livermore National Laboratory. Native NA-LprG was collected to resolution of 2 Å resolution on a Raxis IV++ detector in lab (Rigaku). The data was processed with HKL2000 [38]. The space group of Se-Met NA-LprG was C2 and cell dimensions were a= 95.5 Å , b= 72.3 Å , c= 62.3 Å , α=90 , β=106.8 , r=90 . Native NA-LprG also crystallized in C2 with similar cell dimensions (Table 1). Both had two molecules in an asymmetric unit (molecules A and B). Phases were determined using the Se-Met MAD NA-LprG data set. An initial model from AUTOSHARP [39] was refined with CCP4 REFMAC [40] and PHENIX [41] and built with Coot [42]. The final R_{work} and R_{free} were 22.9% and 27.8% Molecule A is used to represent the structure of NA-LprG in the text.

The crystal structure data for NA-LprG with PIM bound was collected at beamline 23ID-B in Argonne National Lab to a resolution of 1.8 Å (Table 1). HKL2000 was used for data processing. Apo-NA-LprG structure was the template for rigid body refinement with PHENIX. Structure of ligand was built and refined with Coot, CCP4 and PHENIX. The final R_{work} and R_{free} were 22.2% and 25.8%. NA-LprG-V91W crystal data were collected at 19ID in Argonne National Lab. High resolution data was collected to 1.85 Å (Table 1) and

processed with HKL2000 in $P2_1$ space group with cell dimension (a= 39.7 Å , b= 56.0 Å , c= 96.9 Å , α=90 , β=99.6 , r=90). Structure solution was obtained by molecular replacement method [40]. Structure of NA-LprG-V91W was refined with PHENIX and built with Coot. The final R_{work} and R_{free} were 21.5% and 25.3%. Protein structure graphics were produced using the UCSF Chimera [43]. Predicted structure of LprA was generated using CPH model v2.0 (http://www.cbs.dtu.dk/services/CPHmodels/) and MODELLER (http://www.salilab.org/modeller). Cavity sizes of proteins were calculated by using CastP program with spherical probe of 1.4Å [44].

Supplementary Material

Refer to Web version on PubMed Central for supplementary material.

Acknowledgments

We thank Vernon Anderson and Lindsay Sweet for advice and assistance with mass spectrometry, Amy G. Hise (Case Western Reserve University) and Akira Shizuo (Osaka University) for bone marrow from TLR1−/−, TLR6−/− mice, Xuedong Ding, Nancy Nagy and Kitty Daniel for technical assistance, Tracey Musa for comments on the manuscript, and Karen Dobos-Elder and John Belisle (Colorado State University) for Mtb lysates, antibodies and the pVV16 vector. This work was supported by NIH grants AI035726, AI034343 and AI069085 to CVH; HL055967 and AI027243 to WHB; AI071155 and AI049313 to DBM; AI068135 to JCS, the Robert A. Welch Foundation (JCS); the Irvington Institute Fellowship Program of the Cancer Research Institute (CS), American Lung Association grant RG48786N (RER), and the Burroughs Wellcome Fund for Translational Research (DBM and CS). Core facilities of the CWRU Center for AIDS Research were supported by NIH grant AI067093.

References

1. Flynn JL, Chan J. Immunology of tuberculosis. Annu Rev Immunol. 2001; 19:93–129. [PubMed: 11244032]
2. Janeway CA Jr. Approaching the asymptote? Evolution and revolution in immunology. Cold Spring Harb Symp Quant Biol. 1989; 54(Pt 1):1–13. [PubMed: 2700931]
3. Chan J, et al. Microbial glycolipids: possible virulence factors that scavenge oxygen radicals. Proc Natl Acad Sci USA. 1989; 86:2453–2457. [PubMed: 2538841]
4. Fratti RA, Chua J, Vergne I, Deretic V. Mycobacterium tuberculosis glycosylated phosphatidylinositol causes phagosome maturation arrest. Proc Natl Acad Sci USA. 2003; 100:5437–42. [PubMed: 12702770]
5. Vergne I, et al. Mycobacterium tuberculosis phagosome maturation arrest: mycobacterial phosphatidylinositol analog phosphatidylinositol mannoside stimulates early endosomal fusion. Mol Biol Cell. 2004; 15:751–60. [PubMed: 14617817]
6. Cole ST, et al. Deciphering the biology of Mycobacterium tuberculosis from the complete genome sequence. Nature. 1998; 393:537–44. [PubMed: 9634230]
7. Sutcliffe IC, Harrington DJ. Lipoproteins of Mycobacterium tuberculosis: an abundant and functionally diverse class of cell envelope components. FEMS Microbiol Rev. 2004; 28:645–59. [PubMed: 15539077]
8. Bigi F, et al. The knockout of the lprG-Rv1410 operon produces strong attenuation of Mycobacterium tuberculosis. Microbes Infect. 2004; 6:182–7. [PubMed: 14998516]
9. Rengarajan J, Bloom BR, Rubin EJ. Genome-wide requirements for Mycobacterium tuberculosis adaptation and survival in macrophages. Proc Natl Acad Sci U S A. 2005; 102:8327–32. [PubMed: 15928073]
10. Sassetti CM, Rubin EJ. Genetic requirements for mycobacterial survival during infection. Proc Natl Acad Sci U S A. 2003; 100:12989–94. [PubMed: 14569030]
11. Farrow MF, Rubin EJ. Function of a mycobacterial major facilitator superfamily pump requires a membrane-associated lipoprotein. J Bacteriol. 2008; 190:1783–91. [PubMed: 18156250]

12. Sulzenbacher G, et al. LppX is a lipoprotein required for the translocation of phthiocerol dimycocerosates to the surface of Mycobacterium tuberculosis. EMBO J. 2006; 25 :1436–44. [PubMed: 16541102]
13. Jones BW, et al. Different Toll-like receptor agonists induce distinct macrophage responses. J Leukoc Biol. 2001; 69:1036–44. [PubMed: 11404392]
14. Gilleron M, Quesniaux VF, Puzo G. Acylation state of the phosphatidyl inositol hexamannosides from mycobacterium bovis BCG and mycobacterium tuberculosis H37Rv and its implication in TLR response. J Biol Chem. 2003
15. Elass E, et al. Mycobacterial lipomannan induces matrix metalloproteinase-9 expression in human macrophagic cells through a toll-like receptor 1 (TLR1)/TLR2-and CD14-dependent mechanism. Infect Immun. 2005; 73:7064–8. [PubMed: 16177394]
16. Tapping RI, Tobias PS. Mycobacterial lipoarabinomannan mediates physical interactions between TLR1 and TLR2 to induce signaling. J Endotoxin Res. 2003; 9:264–8. [PubMed: 12935358]
17. Bhatt K, Salgame P. Host innate immune response to Mycobacterium tuberculosis. J Clin Immunol. 2007; 27:347–62. [PubMed: 17364232]
18. Pai RK, Convery M, Hamilton TA, Boom WH, Harding CV. Inhibition of IFN-gamma-induced class II transactivator expression by a 19-kDa lipoprotein from Mycobacterium tuberculosis: a potential mechanism for immune evasion. J Immunol. 2003; 171:175–184. [PubMed: 12816996]
19. Noss EH, et al. Toll-like receptor 2-dependent inhibition of macrophage class II MHC expression and antigen processing by 19 kD lipoprotein of Mycobacterium tuberculosis. J Immunol. 2001; 167:910–918. [PubMed: 11441098]
20. Brightbill HD, et al. Host defense mechanisms triggered by microbial lipoproteins through toll-like receptors. Science. 1999; 285:732–736. [PubMed: 10426995]
21. Takeuchi O, et al. Cutting edge: role of Toll-like receptor 1 in mediating immune response to microbial lipoproteins. J Immunol. 2002; 169:10–4. [PubMed: 12077222]
22. Nigou J, et al. Mannan chain length controls lipoglycans signaling via and binding to TLR2. J Immunol. 2008; 180:6696–702. [PubMed: 18453589]
23. Pecora ND, Gehring AJ, Canaday DH, Boom WH, Harding CV. Mycobacterium tuberculosis LprA is a lipoprotein agonist of TLR2 that regulates innate immunity and APC function. J Immunol. 2006; 177:422–429. [PubMed: 16785538]
24. Gehring AJ, Dobos KM, Belisle JT, Harding CV, Boom WH. Mycobacterium tuberculosis LprG (Rv1411c): A novel TLR-2 ligand that inhibits human macrophage class II MHC antigen processing. J Immunol. 2004; 173:2660–8. [PubMed: 15294983]
25. Jung SB, et al. The mycobacterial 38-kilodalton glycolipoprotein antigen activates the mitogen-activated protein kinase pathway and release of proinflammatory cytokines through Toll-like receptors 2 and 4 in human monocytes. Infect Immun. 2006; 74 :2686–96. [PubMed: 16622205]
26. Jin MS, et al. Crystal structure of the TLR1-TLR2 heterodimer induced by binding of a tri-acylated lipopeptide. Cell. 2007; 130:1071–82. [PubMed: 17889651]
27. Rezwan M, Grau T, Tschumi A, Sander P. Lipoprotein synthesis in mycobacteria. Microbiology. 2007; 153:652–8. [PubMed: 17322184]
28. Nigou J, Gilleron M, Puzo G. Lipoarabinomannans: characterization of the multiacylated forms of the phosphatidyl-myo-inositol anchor by NMR spectroscopy. Biochem J. 1999; 337 (Pt 3):453–60. [PubMed: 9895288]
29. Bigi F, et al. The gene encoding P27 lipoprotein and a putative antibiotic-resistance gene form an operon in Mycobacterium tuberculosis and Mycobacterium bovis. Microbiology. 2000; 146 (Pt 4):1011–8. [PubMed: 10784059]
30. Gilleron M, Nigou J, Nicolle D, Quesniaux V, Puzo G. The acylation state of mycobacterial lipomannans modulates innate immunity response through toll-like receptor 2. Chem Biol. 2006; 13:39–47. [PubMed: 16426970]
31. Kang JY, et al. Recognition of Lipopeptide Patterns by Toll-like Receptor 2-Toll-like Receptor 6 Heterodimer. Immunity. 2009
32. Berg S, Kaur D, Jackson M, Brennan PJ. The glycosyltransferases of Mycobacterium tuberculosis -roles in the synthesis of arabinogalactan, lipoarabinomannan, and other glycoconjugates. Glycobiology. 2007; 17:35–56R. [PubMed: 17261566]

33. Finberg RW, Re F, Popova L, Golenbock DT, Kurt-Jones EA. Cell activation by Toll-like receptors: role of LBP and CD14. J Endotoxin Res. 2004; 10:413–8. [PubMed: 15588424]
34. Jiang Z, et al. CD14 is required for MyD88-independent LPS signaling. Nat Immunol. 2005; 6:565–70. [PubMed: 15895089]
35. Sklar MD, Tereba A, Chen BD, Walker WS. Transformation of mouse bone marrow cells by transfection with a human oncogene related to c-myc is associated with the endogenous production of macrophage colony stimulating factor 1. J Cell Physiol. 1985; 125:403–12. [PubMed: 3877730]
36. Flo TH, et al. Involvement of toll-like receptor (TLR) 2 and TLR4 in cell activation by mannuronic acid polymers. J Biol Chem. 2002; 277:35489–95. [PubMed: 12089142]
37. Latz E, et al. Lipopolysaccharide rapidly traffics to and from the Golgi apparatus with the toll-like receptor 4-MD-2-CD14 complex in a process that is distinct from the initiation of signal transduction. J Biol Chem. 2002; 277:47834–43. [PubMed: 12324469]
38. Otwinowski Z, Minor W. Processing of X-ray diffraction data collected in oscillation mode. Methods Enzymol. 1997; 276:307–326.
39. Vonrhein C, Blanc E, Roversi P, Bricogne G. Automated structure solution with autoSHARP. Methods Mol Biol. 2007; 364:215–30. [PubMed: 17172768]
40. Murshudov GN, Vagin AA, Dodson EJ. Refinement of macromolecular structures by the maximum-likelihood method. Acta Crystallogr D Biol Crystallogr. 1997; 53 :240–55. [PubMed: 15299926]
41. Adams PD, et al. PHENIX: building new software for automated crystallographic structure determination. Acta Crystallogr D Biol Crystallogr. 2002; 58:1948–54. [PubMed: 12393927]
42. Emsley P, Cowtan K. Coot: model-building tools for molecular graphics. Acta Crystallogr D Biol Crystallogr. 2004; 60:2126–32. [PubMed: 15572765]
43. Pettersen EF, et al. UCSF Chimera--a visualization system for exploratory research and analysis. J Comput Chem. 2004; 25:1605–12. [PubMed: 15264254]
44. Dundas J, et al. CASTp: computed atlas of surface topography of proteins with structural and topographical mapping of functionally annotated residues. Nucleic Acids Res. 2006; 34:W116–8. [PubMed: 16844972]

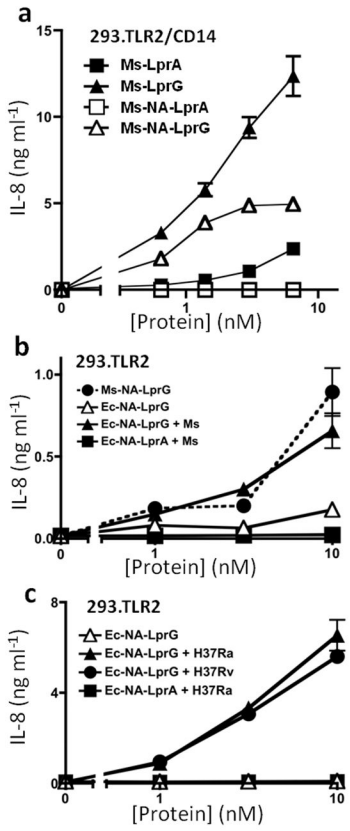

Fig. 1. NA-LprG carries a mycobacterial TLR2 agonist

(A) HEK293.TLR2/CD14 cells show a dose-dependent IL-8 response to LprA, LprG, and NA-LprG, but no response to NA-LprA. Control HEK293 cells lacking TLR2 and CD14 failed to respond to all four proteins (data not shown). Absence of CD14 (HEK293.TLR2 cells) reduced the apparent potency of NA-LprG but not acylated LprG or LprA (Supplemental Fig. S-1). (B, C) NA-LprG can acquire TLR2 agonist activity from mycobacterial lysates. NA-LprG and NA-LprA were expressed in *E. coli*, purified by Ni-affinity and anion-exchange chromatography, incubated with control buffer or a lysate of *M. smegmatis* (B), Mtb H37Ra (C) or Mtb H37Rv (C), repurified by Ni-affinity (B) or Ni-affinity and ion exchange chromatography (C), and incubated with HEK293.TLR2 cells for 12 h. Minor technical differences between the panels resulted in different plateau IL-8 levels, but this was not due to intrinsic differences in activities of materials from *M. smegmatis* vs. Mtb (Fig. 3 and data not shown). HEK293.TLR2/CD14 cells used in panel A give higher IL-8 secretion responses than HEK293.TLR2 cells used in panels B and C (see Supplemental Fig. S-1). For all data panels, IL-8 production was quantified by ELISA, and data are reported as the mean +/− SD of triplicate HEK293.TLR2 assays. Results are representative of at least 3 independent experiments.

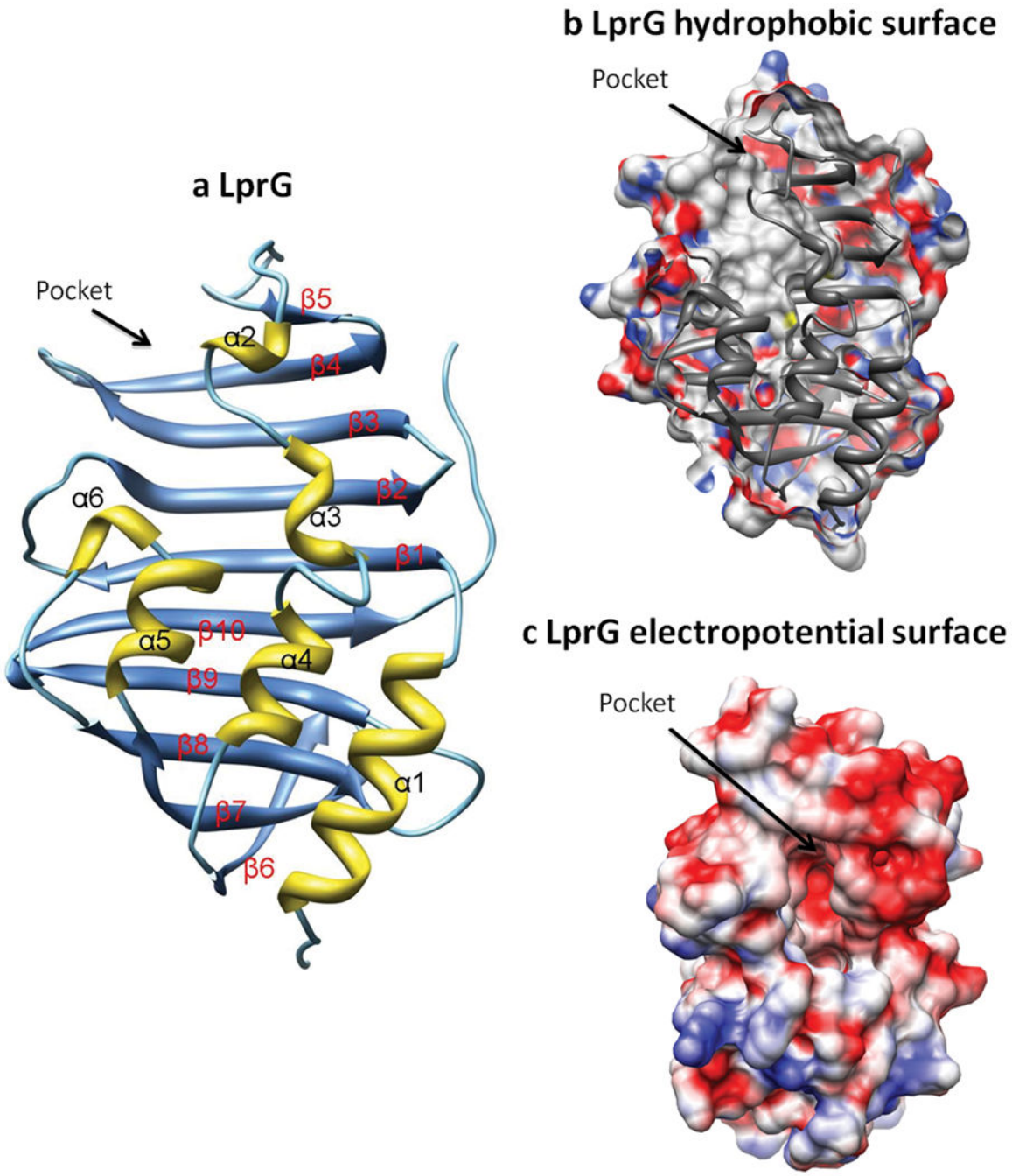

Fig. 2. Crystal structure of NA-LprG reveals a hydrophobic pocket with the potential to carry a TLR2 agonist

(A) LprG structure viewed in ribbons. (B) LprG hydrophobic surface slab view clipped to cavity center (carbon in white, oxygen in red, nitrogen in blue and sulfur in yellow). (C) Electrostatic surface view of the LprG cavity entrance (negative in red, positive in blue, neutral in white). In order to show the entrance, LprG is rotated 90 to the right and 30 down relative to the other views. The cavity entrance is located between β-sheet and α-helices.

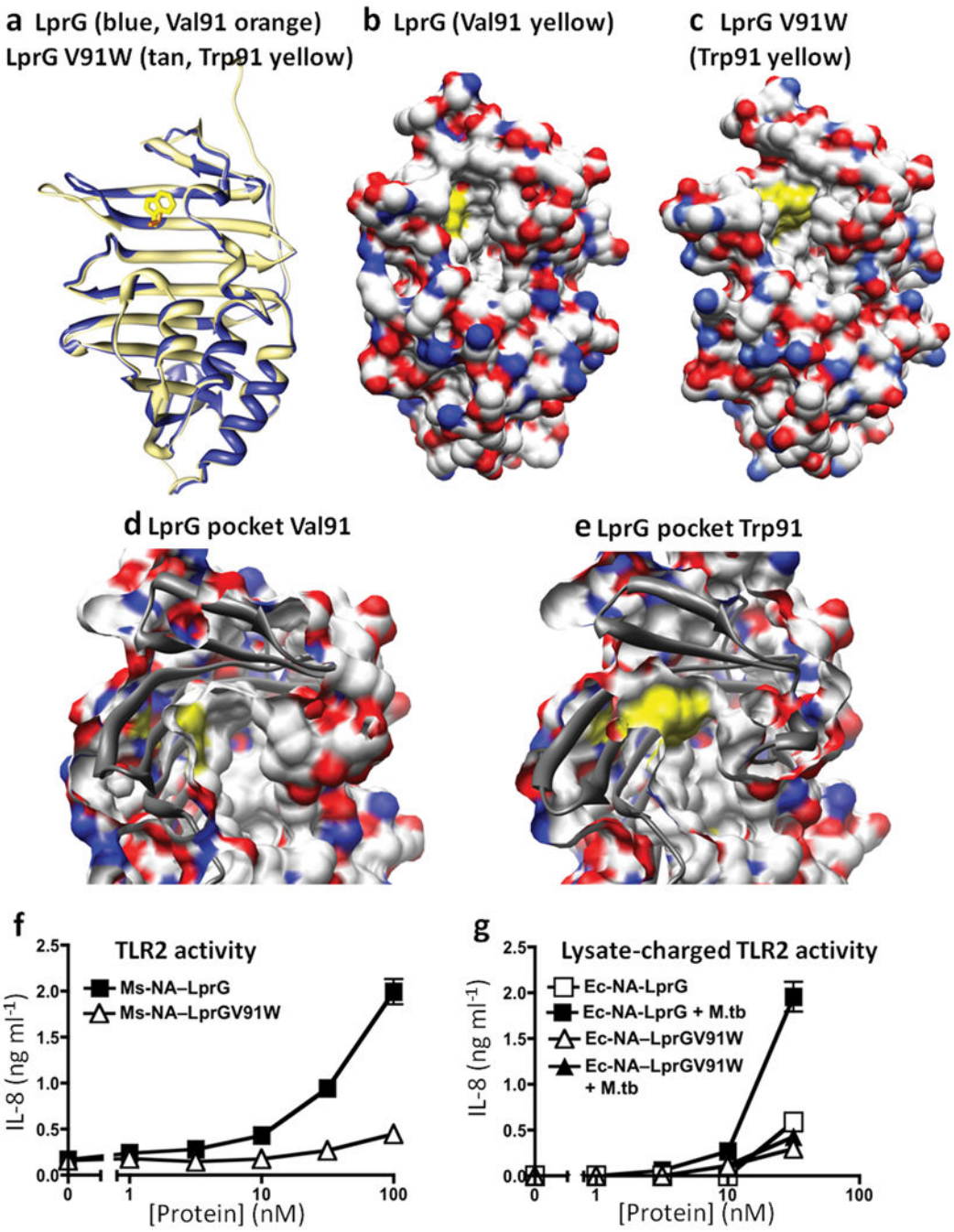

Fig. 3. Site-directed mutagenesis to alter the structure of the NA-LprG pocket and binding of TLR2 agonists

(A) Superimposition ribbon view of NA-LprG (blue, V91 in orange) and mutant NA-LprG-V91W (tan, W91 in yellow). In addition to the V91W mutation, NA-LprG and NA-LprG-V91W constructs used for crystallization included minor differences unrelated to the pocket structure (e.g. NA-LprG-V91W has a longer C-terminal coil). Otherwise, overall structures were similar with differences due to the V91W mutation localized to the cavity and entrance. Movement of β3, β4 and the loop between β3 and β4 affects cavity and entrance size. (B) Hydrophobic view of the NA-LprG entrance (white, carbon; red, oxygen; blue,

nitrogen; yellow, V91). (C) Hydrophobic view of NA-LprG-V91W (yellow, W91). The extra C-terminal coil of NA-LprG-V91W was removed for better surface comparison. The V91W mutation causes the cavity wall to shift by 3.5 Å. (D) View revealing hydrophobic surface of the NA-LprG cavity. (E) NA-LprG-V91W cavity. The V91W mutation narrows the pocket to reduce space of ligand binding. (F) TLR2 activity of NA-LprG and NA-LprG-V91W expressed in *M. smegmatis* and tested on HEK293.TLR2 cells. (G) TLR2 activity of NA-LprG and NA-LprG-V91W expressed in *E. coli*, purified, incubated with Mtb H37Ra or H37Rv lysate and repurified. Data are reported as mean +/− SD of triplicate HEK293.TLR2 assays.

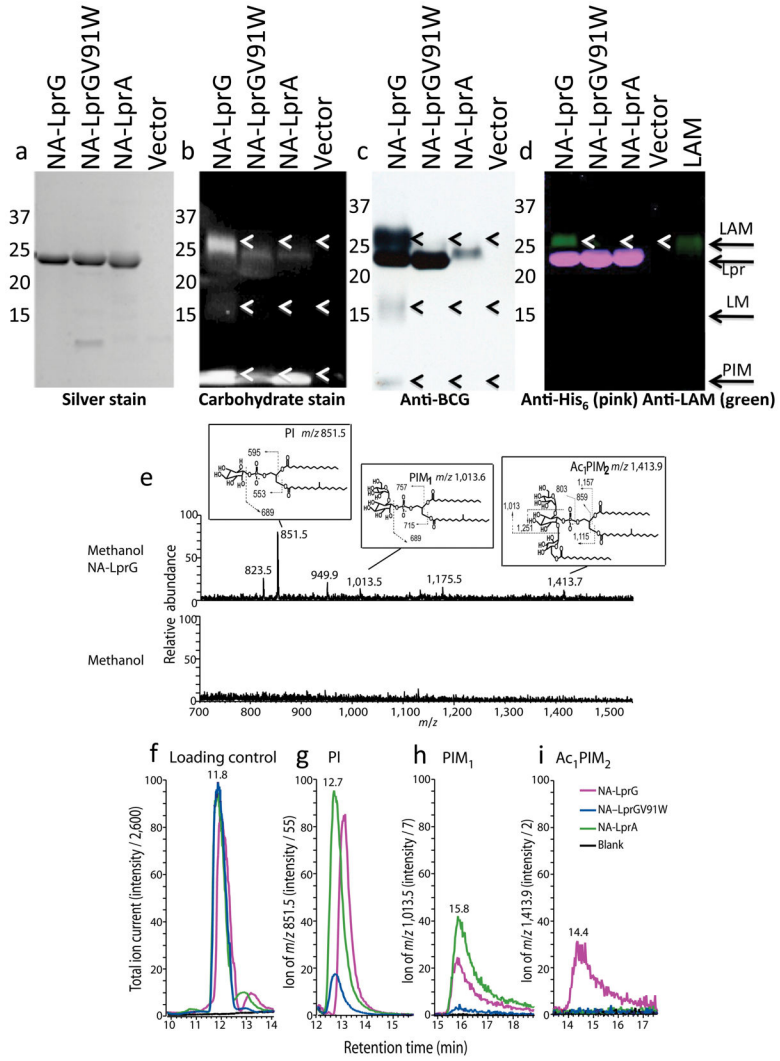

Fig. 4. Triacylated mycobacterial glycolipids are associated with NA-LprG

(A-D) SDS-PAGE analysis of proteins purified from *M. smegmatis*. Samples were visualized by silver stain (A), Pro-Q stain for carbohydrates (B), polyclonal anti-BCG Western blot (C), and monoclonal anti-His_6 [pink] and anti-LAM [green] (D). The 10-kDa molecular weight marker ran at the gel dye front. Arrows on right that are labeled LAM, LM and PIM represent the positions observed with glycolipid standards run in this gel system. Arrowheads within the gels indicate the expected positions for LAM, LM and PIM whether or not those species are present. See supplemental methods. (E) Negative mode electrospray ionization mass spectrometry of methanol-treated NA-LprG yielded ions corresponding in mass to mycobacterial phospholipids. Ions of *m/z* 851.5, 1013.5 and 1413.7 were subjected to negative mode collision induced dissociation mass spectrometry, yielding ions that corresponded to masses and fragments indicated in the insets and Fig. S-2. Ions detected near *m/z* 823.5 correspond to an alternately acylated form of phosphatidylinositol, and ions detected near *m/z* 949.9 correspond to an H_3PO_4 adduction of phosphatidylinositol. Ions detected near 1175.5 correspond to diacylated PIM2. (F-I) LC-MS analysis was carried out on 4.3 nanomoles of NA-LprG (pink), NA-LprG-V91W (blue), NA-LprA (green) and

solvent blank (black). The total ion current trace shows that signals from non-lipidic components of protein preparations were detected at similar levels, serving as a control for equivalent loading of proteins onto the column (F). Mass chromatograms measured in narrow mass ranges corresponding to the masses of phosphatidylinositol (*m/z* 851.5) (G) diacyl PIM_1 (*m/z* 1013.6) (H), and triacyl Ac_1PIM_2 (*m/z* 1413.76) (I) are shown.

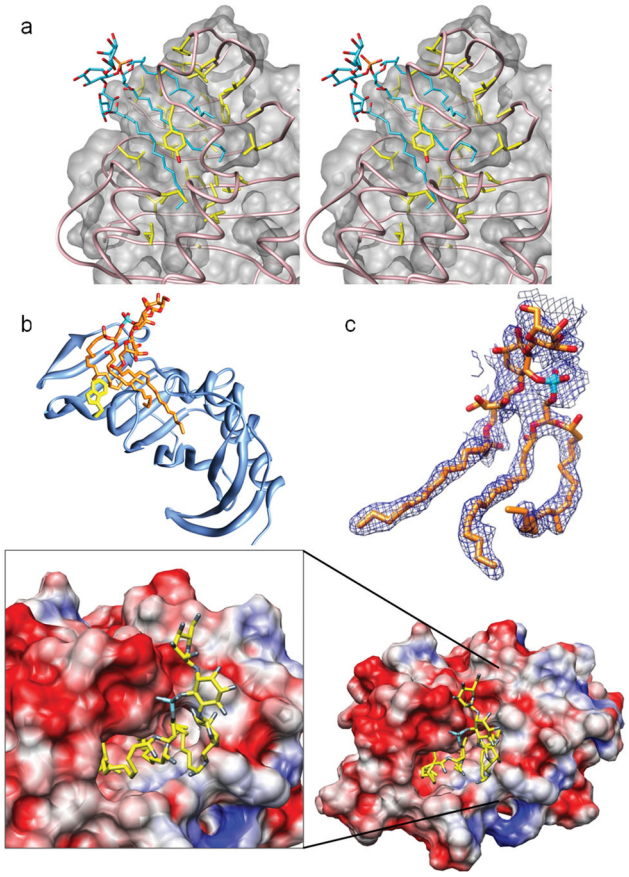

Fig. 5.

Crystal structure of Ac_1PIM_2 bound to NA-LprG.

(A) Ac_1PIM_2 (in cyan) bound to NA-LprG (stereo pair image). Residues (in yellow) in the cavity interact with Ac_1PIM_2. The cavity provides enough space for the tri-acyl chains of Ac_1PIM_2. (B) Structure of Ac_1PIM_2 from NA-LprG-Ac_1PIM_2 (in orange) superimposed onto the structure of NA- LprG-V91W (blue, W91 in yellow). Tryptophan 91 hinders a part of the binding pocket that accommodates one of the Ac_1PIM_2 acyl chains. (C) Electron density of $2F_o$-F_c map at 1 sigma level for Ac_1PIM_2 as bound to NA-LprG. (D) View of the cavity entrance with a close-up (colored according to surface electrostatic potential with Ac_1PIM_2 in yellow). The sugar moieties of Ac_1PIM_2 are bound closely to a negatively charged site on the LprG surface.

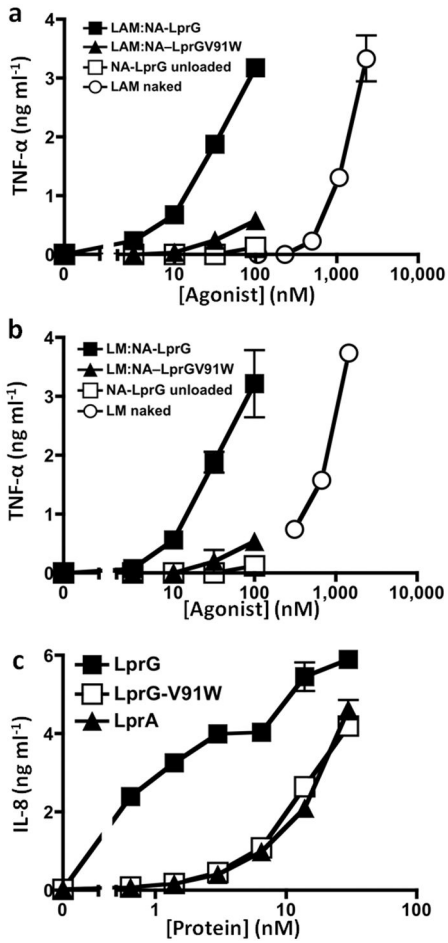

Fig. 6. LprG binds purified mycobacterial glycolipids and facilitates their recognition by TLR2

(A, B) NA-LprG was purified from *E. coli*, incubated with LAM or LM from *M. smegmatis*, repurified and assessed for TLR2 activity using bone marrow-derived macrophages. TNF-alpha production was quantified by ELISA. “LAM:NA-LprG” represents NA-LprG that was incubated with LAM and repurified; “NA-LprG unloaded” represents NA-LprG that was sham-loaded with buffer and repurified; and “Naked LAM” represents glycolipid in the absence of NA-LprG. Data are reported as mean +/− SD of triplicate macrophage assays. (C) Acylated LprG, LprA, and LprG-V91W were purified from *M. smegmatis* and assessed for TLR2 agonist activity with HEK293.TLR2-CD14 as in Fig. 1. Data are reported as mean +/− SD of triplicate HEK293.TLR2-CD14 assays.

Table 1

Data collection, phasing and refinement statistics for MAD (SeMet) structures

	Native NA-LprG	SeMet NA-LprG			LprG-V91W	LprG-PIM
Data collection						
Space group	C2	C2			$P2_1$	C2
Cell dimensions						
a, *b*, *c* (Å)	95.3, 71.9, 61.3	95.5 72.3 62.3			39.7, 56.0, 96.9	95.3, 71.9, 61.3
α, β, γ(°)	90.0, 106.3, 90.0	90.0 106.8 90.0			90.0, 99.5, 90.0	90.0, 106.3, 90.0
		Peak	*Inflection*	*Remote*		
Wavelength	1.5418	0.9796	0.9798	0.9537	0.9794	0.9795
Resolution (Å)	2.0 (2.07–2.00)	1.9 (1.97–1.90)	1.9 (1.97–1.90)	1.9 (1.97–1.90)	1.8 (1.82–1.8)	1.85 (1.92–1.85)
R_{sym} or R_{merge}	0.068 (0.73)	0.076 (0.57)	0.057 (0.41)	0.061 (0.53)	0.063 (0.59)	0.068 (0.72)
I / σI	461.1 (13.7)	42.5 (2.4)	80.3 (4.1)	55.0 (3.0)	42.7 (2.3)	256.6 (5.5)
Completeness (%)	98.7	90.6	98.1	94.5	97.0 (98.5)	99.9 (99.8)
Redundancy	7.5	6.6	7.2	6.9	2.8 (2.7)	5.7 (5.2)
Refinement						
Resolution (Å)	50.0–2.0				50.0–1.8	50.0–1.85
No. reflections	811524				696007	469056
R_{work} / R_{free}	22.90/27.8				21.5/25.3	22.2/25.8
No. atoms						
Protein	2874				3030	2876
Ligand/ion	0				N/A	97
Water	114				479	175
B-factors						
Protein	49.8				26.0	43.2
Ligand	N/A				N/A	63.2
Water	49.1				33.5	44.0
R.m.s deviations						
Bond lengths (Å)	0.008				0.006	0.007
Bond angles (°)	1.152				1.058	1.144

*Values in parentheses are for highest-resolution shell.